SUPPLEMENTARY MATERIALS FOR:

Flagellar structures from the bacterium *Caulobacter crescentus* and implications for phage ΦCbK predation of multi-flagellin bacteria.

Eric J. Montemayor[a,b†], Nicoleta T. Ploscariu[a†], Juan C. Sanchez[a,c,‡], Daniel Parrell[a,‡], Rebecca S. Dillard[d], Conrad W. Shebelut[e], Zunlong Ke[d,f], Ricardo C. Guerrero-Ferreira[d], and Elizabeth R. Wright[a,b,c,d,g,#]

[a]Department of Biochemistry, University of Wisconsin, Madison, WI 53706

[b]Cryo-Electron Microscopy Research Center, Department of Biochemistry, University of Wisconsin, Madison, WI 53706

[c]Biophysics Graduate Program, University of Wisconsin, Madison, WI 53706

[d]Division of Infectious Diseases, Department of Pediatrics, Emory University School of Medicine, Children's Healthcare of Atlanta, Atlanta, GA, 30322

[e]Department of Pathology and Laboratory Medicine, Emory University School of Medicine, Atlanta, GA, 30322

[f]School of Biological Sciences, Georgia Institute of Technology, Atlanta, GA, 30332

[g]Morgridge Institute for Research, Madison, WI, 53715

[†]These authors contributed equally. Author order was determined alphabetically.

[‡]These authors contributed equally. Author order was determined in order of increasing seniority.

#To whom correspondence should be addressed. E-mail: erwright2@wisc.edu

SUPPLEMENTARY TEXT

Helical reconstruction in the absence of *de novo* indexing

Helical reconstruction relies upon *de novo* indexing and acquisition of helical symmetry parameters, a process that is labor intensive and not always readily achievable (1). As such, the current state of helical reconstruction methods very much resembles that of macromolecular X-ray crystallography several decades ago, specifically the requirement for experimental phase determination (2). Here we demonstrate that utilizing prior knowns from homologous structures can greatly accelerate the path to structure determination. More specifically, we have employed something akin to "helical molecular replacement" to obtain initial estimates for helical symmetry from homologous structures to kick-start our reconstructions (3, 4). This approach to helical reconstruction is similarly fraught with biases that can potentially yield false "solutions" for structure determination (5). As such, cross-validation metrics are essential to the pipeline we have employed here. The primary metric we have relied upon is the appearance of high resolution structural features in our final reconstructions that comport with known stereochemistry and other features of protein structure (Fig. 5B). Furthermore, we also confirmed that observed amplitude spectra from 2-D classification before application of helical reconstruction are qualitatively similar to those derived from projections of the reconstructed maps. (Fig. S5B). As an additional validation metric, we compared refined out-of-plane tilt values for all particle stacks that were used for reconstruction (Fig. S6). Refinement of the straightened FljK particle stack with likely incorrect symmetry gives a nonsensical map (Fig. S6A) with a pronounced bi-modal distribution of out-of-plane tilts values. Using this same analysis on the straightened FljK particle stack with our estimated

symmetry (Fig. S6B) returns a near gaussian distribution of out-of-plane tilt values, while the non-straightened FljK and FljK/L reconstructions are nearly gaussian with a small dip about the median (Figs. S6C,D), which is far less pronounced than that observed for the likely incorrect symmetry test case above (Fig. S6A). The small deviation from a gaussian distribution likely arises from the non-straightened nature of the corresponding filaments and therefore imperfect application of helical symmetry.

Our ability to generate a reconstruction of a non-straightened FljK flagellum shows that conformational heterogeneity does not necessarily preclude structure determination of flagellar filaments by helical reconstruction methods, similar to recent work by Blum *et al*. (6). We note that map quality is globally degraded in the presence of conformational heterogeneity, and the "best" region of the map becomes more strongly restricted to the center of the reconstruction as conformational heterogeneity increases (Fig. 5C). Excessive conformational heterogeneity can make helical reconstruction impossible, and in such cases conventional single particle reconstructions must instead be utilized (7). However, the latter approach is typically only feasible for larger asymmetric units and, as expected, our attempts to use standard single particle methods on our filaments failed (data not shown) (5).

In comparing our three reconstructions, it is apparent that the combination of compositional and conformational heterogeneity significantly impedes high resolution structure determination. For example, the non-straightened FljK and FljKL filaments exhibit similar curvature (Fig. 5A), yet only the compositionally homogeneous FljK filament yielded a three-dimensional map of sufficient quality to generate an atomic model. One possibility for the limitation of FljKL could be that the highly similar, yet

distinct, flagellin monomers are stochastically incorporated throughout the body of the filament, and as such the resulting numerous combinatorial possibilities preclude significant accumulation of any one single composition for averaging *in silico*.

SUPPLEMENTARY FIGURES

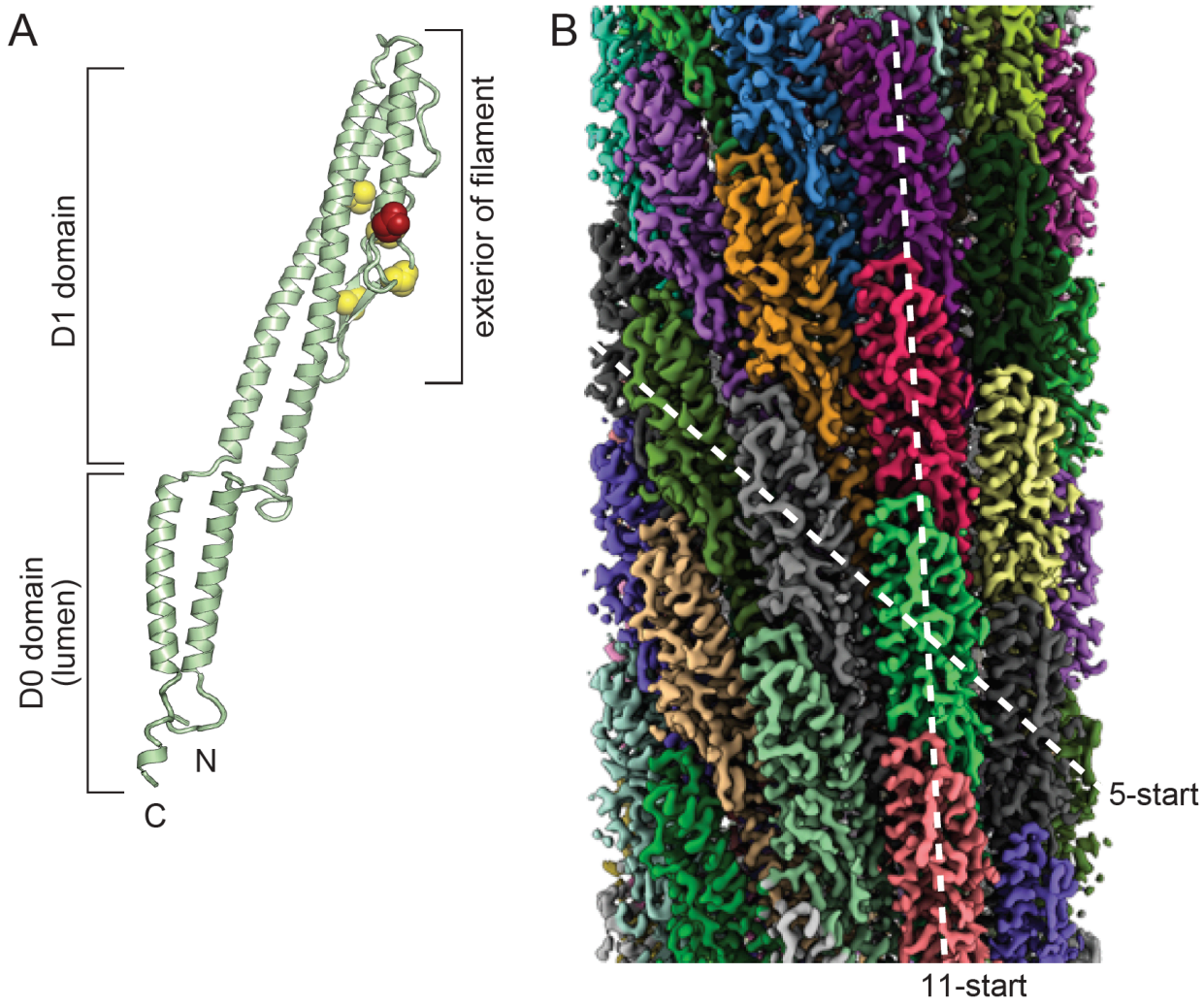

Supplementary Figure 1. Architecture of flagellins. A) Each monomer has N-terminal and C-terminal helices that make up the D0 domains at the center of the filament, a pair of adjacent helices that comprise the D1 domain, and between the D1 helices is an insertion region that is exposed to the surface of the filament. Shown here is the FljK flagellin. Post-translationally modified residues are depicted by yellow spheres and the N130S straightening substitution used in this work is shown by red spheres. B) Schematic of the *C. crescentus* FljK filament, with different colors for adjacent flagellin monomers. The 5-start and 11-start protofilaments are annotated in the image with dashed lines.

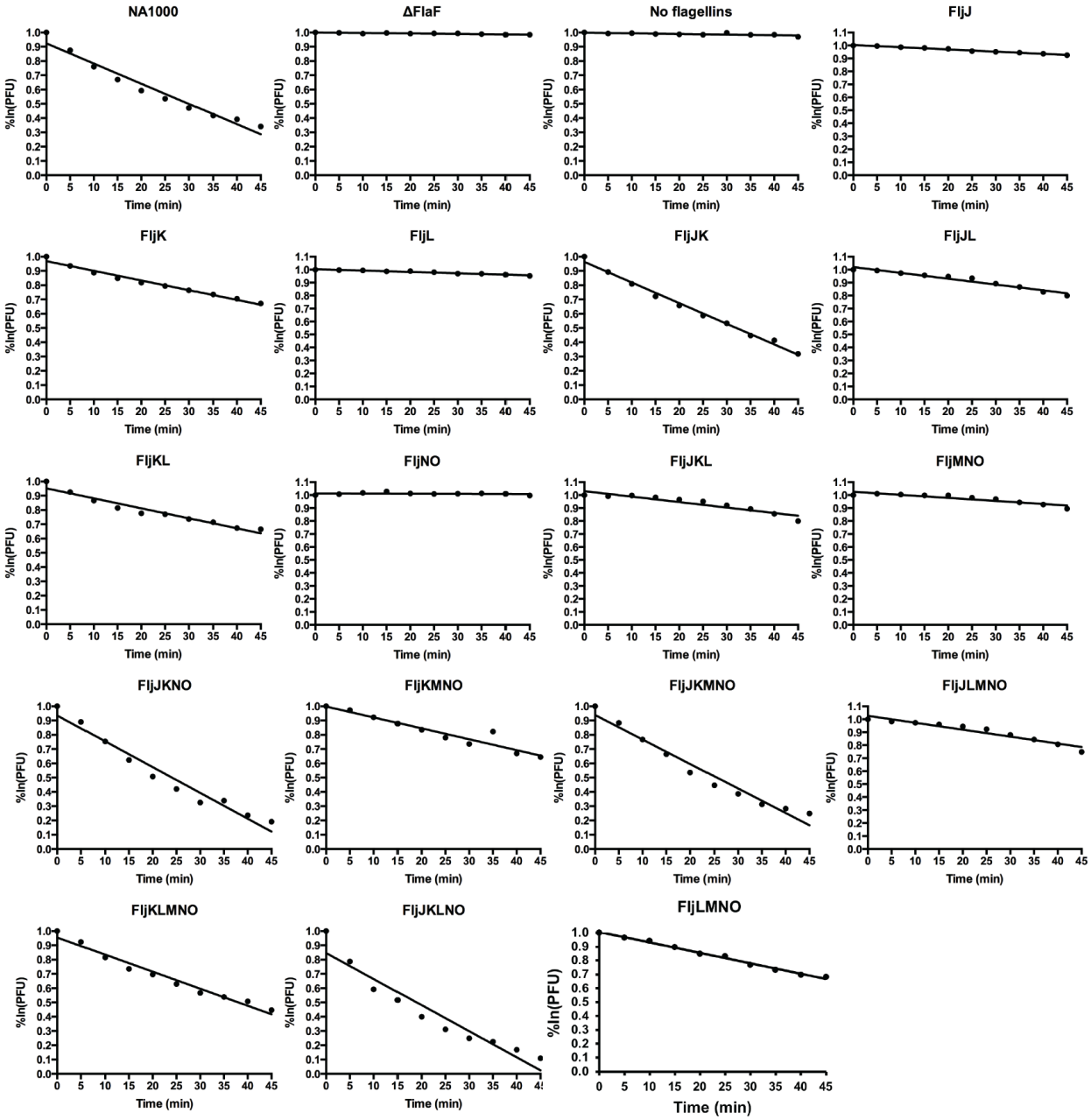

Supplementary Figure 2. Adsorption kinetics of phage ϕCbK to *C. crescentus* strains with altered flagellin complements. Data points represent the natural logarithm of phage titer relative to the initial titer at time 0 [$\ln(T_t/T_{t=0})$].

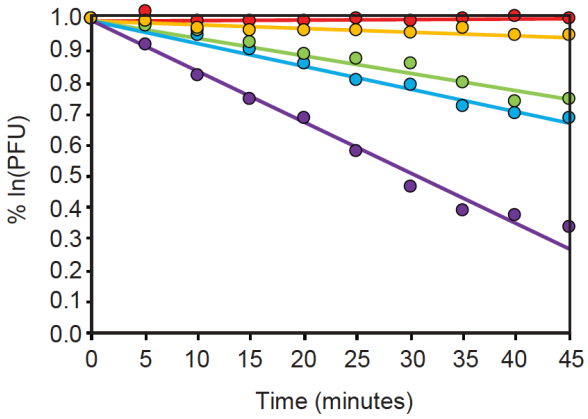

strain	ΦCbK adsorption	motility
no flagellins	0.0 %	7.3 %
FljK-T103C/N130S only (CS12)	7.8 %	11 %
FljK only	47 %	46 %
FljK-T103C only (CS3)	57 %	37 %
all flagellins (NA1000)	100 %	100 %

Supplementary Figure 3. Adsorption kinetics of phage ϕCbK to *C. crescentus* strains with point mutations in FljK. Data points represent the natural logarithm of phage titer relative to the initial titer at time 0 [$\ln(T_t/T_{t=0})$].

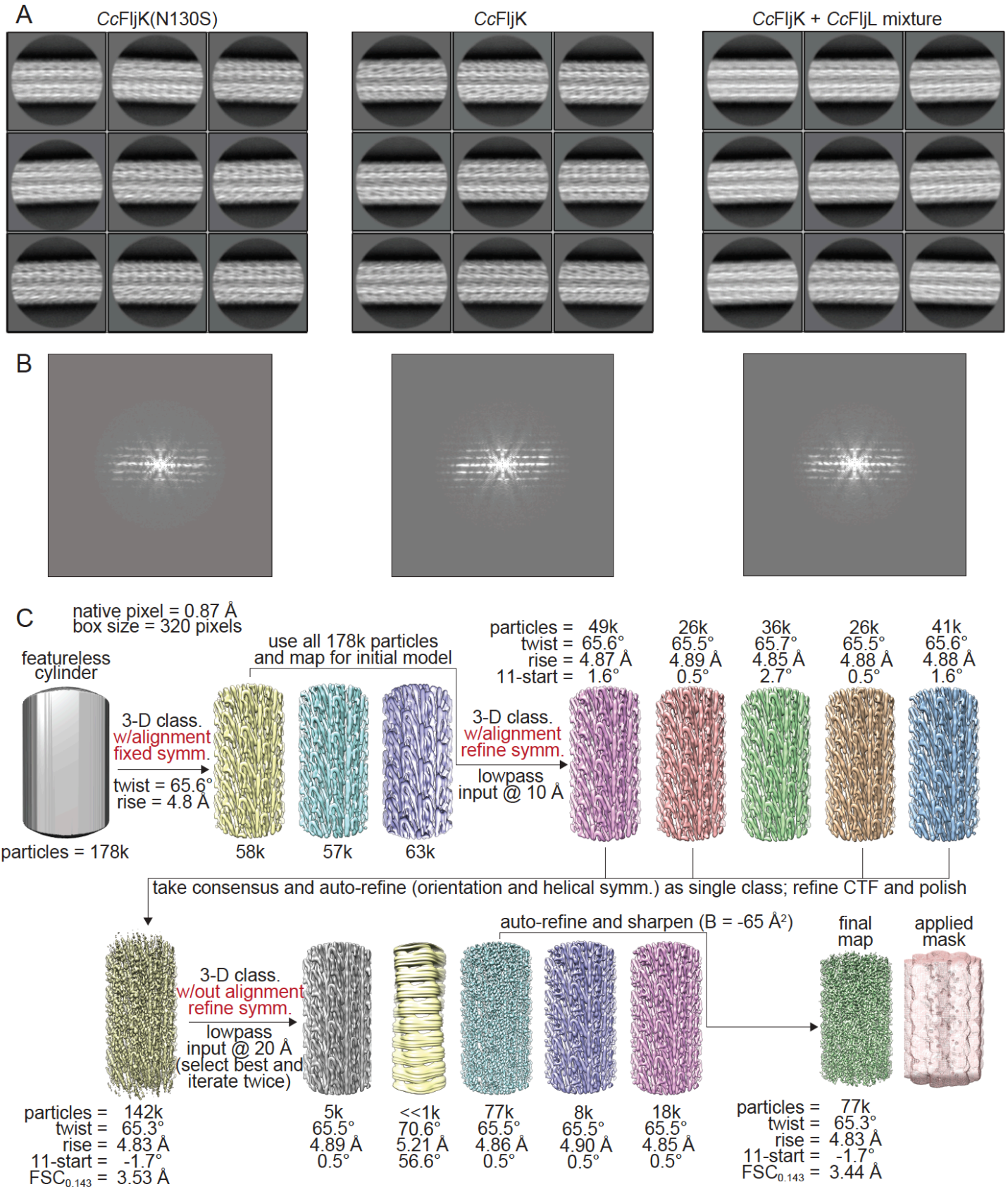

D

initial model:

```
`which relion_refine_mpi` --o Class3D/job011/run --i Extract/job010/particles.star --ref 320-pix-cylinder-bin2x.mrc --firstiter_cc --ini_high
60 --dont_combine_weights_via_disc --pool 30 --pad 2  --ctf --iter 20 --tau2_fudge 4 --particle_diameter 250 --fast_subsets  --K 3 --flatten_-
solvent --zero_mask --oversampling 1 --healpix_order 3 --offset_range 20 --offset_step 2 --sym C1 --norm --scale  --helix --helical_inner_di-
ameter 10 --helical_outer_diameter 150 --helical_nr_asu 1 --helical_twist_initial 65.6 --helical_rise_initial 4.8 --helical_z_percentage 0.5
--helical_keep_tilt_prior_fixed --sigma_tilt 5 --sigma_psi 3.33333 --sigma_rot 0 --j 2 --gpu ""  --pipeline_control Class3D/job011/
```

Supplementary Figure 4. Helical reconstruction in the Relion 3.1 framework. A) Example 2-D classes. B) Representative amplitude spectra from initial 2-D classes. Although the spectra are not of sufficient quality for *de novo* determination of helical symmetry, the observed layer line spacing is consistent with a helical repeat that is similar to that in homologous flagellins of known structure (6, 8-10) (Fig. S5). C) Helical reconstruction using initial helical symmetry values from homologous flagellins. After generation of an initial model, the helical symmetry values are further refined to yield a high-resolution structure. Using this pipeline, the FljK-only flagellins give reconstructions in the low 3 Å resolution range, whereas the heterogeneous FljK/L flagellin is trapped at ~ 4.6 Å. D) Example command used for initial model generation in Relion 3.1.

A

*Cc*FljK
before reconstuction

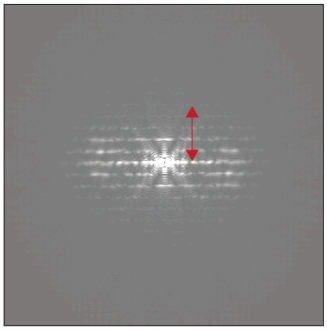

B

*Cc*FljK
after reconstuction

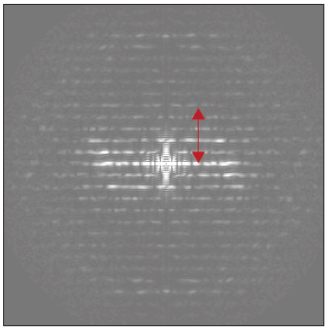

5 layer lines ~ 53 pixels

$$\text{helical repeat} = \frac{2*\text{pixel}*\text{box}}{\text{pixels per layer line}}$$

$$\text{helical repeat} = \frac{2*1.74\ \text{Å}*160\ \text{pixel}}{10\ \text{pixels}}$$

helical repeat = ~ 53 Å

C

*Cc*FljK
after reconstuction
helical plot using refined symm.

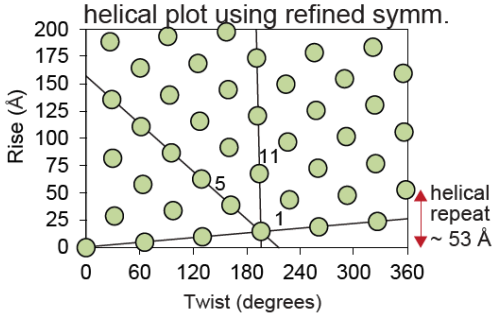

*Cc*FljK - N130S variant
before reconstuction

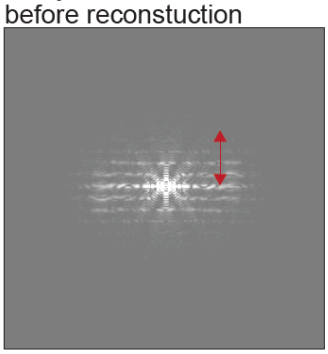

*Cc*FljK - N130S variant
after reconstuction

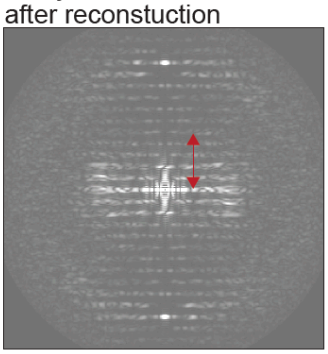

5 layer lines ~ 53 pixels

$$\text{helical repeat} = \frac{2*\text{pixel}*\text{box}}{\text{pixels per layer line}}$$

$$\text{helical repeat} = \frac{2*1.74\ \text{Å}*160\ \text{pixel}}{10.6\ \text{pixels}}$$

helical repeat = ~ 53 Å

*Cc*FljK - N130S variant
after reconstuction
helical plot using refined symm.

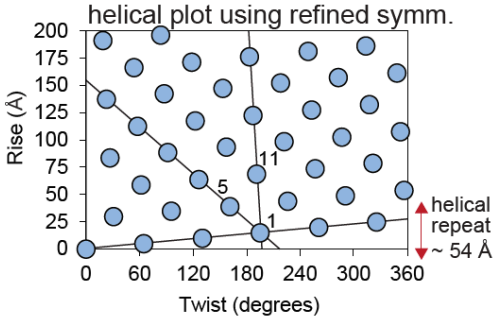

*Cc*FljK + *Cc*FljL mixture
before reconstuction

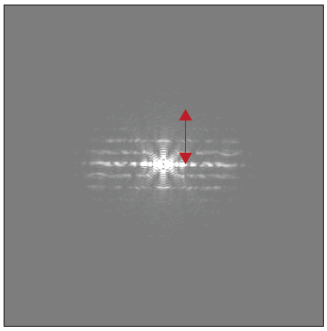

*Cc*FljK + *Cc*FljL mixture
after reconstuction

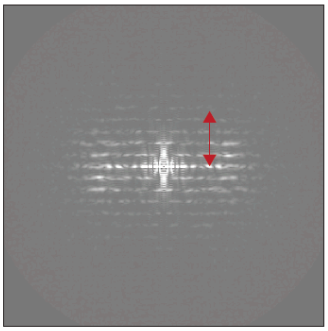

5 layer lines ~ 54 pixels

$$\text{helical repeat} = \frac{2*\text{pixel}*\text{box}}{\text{pixels per layer line}}$$

$$\text{helical repeat} = \frac{2*1.74\ \text{Å}*160\ \text{pixel}}{10.8\ \text{pixels}}$$

helical repeat = ~ 52 Å

*Cc*FljK + *Cc*FljL mixture
after reconstuction
helical plot using refined symm.

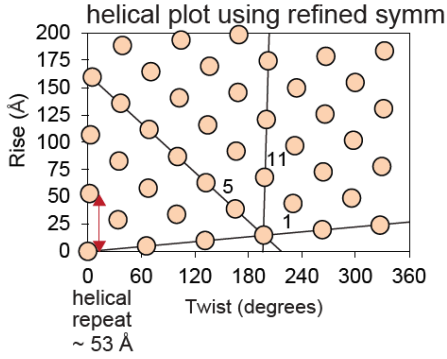

D

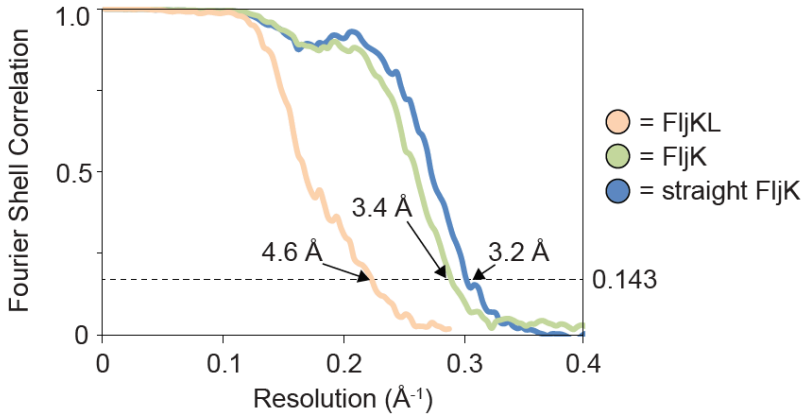

Supplementary Figure 5. Comparison of amplitude spectra before and after helical reconstruction. A,B) Representative amplitude spectrum from a naïve 2-D classification is similar to that obtained from reconstructed maps after application of helical symmetry in Relion 3.1. In both cases, the observed repeat distance is ~ 56 Å. C) When viewed in a helical plot, the refined rise and twist from reconstruction gives a similar repeat distance of ~ 53 Å. D) Masked FSC curves for the three reconstructions presented here.

A

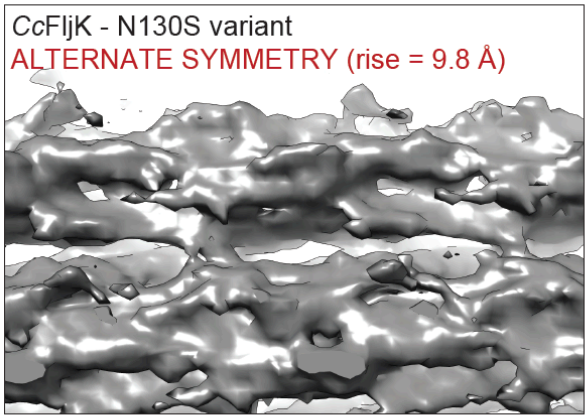
*Cc*FljK - N130S variant
ALTERNATE SYMMETRY (rise = 9.8 Å)

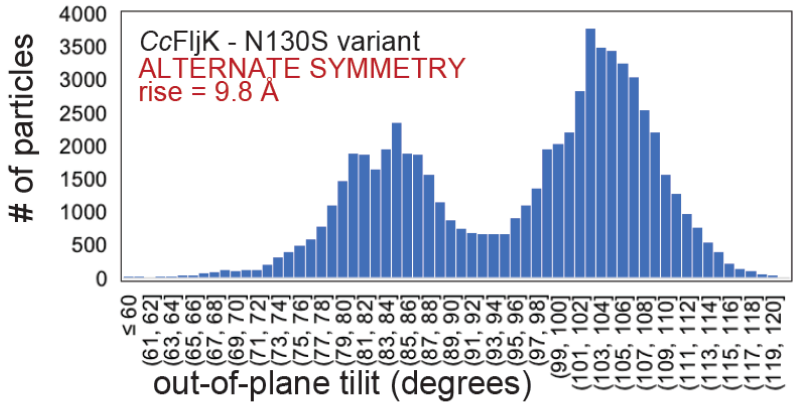
*Cc*FljK - N130S variant
ALTERNATE SYMMETRY
rise = 9.8 Å
# of particles
out-of-plane tilit (degrees)

B

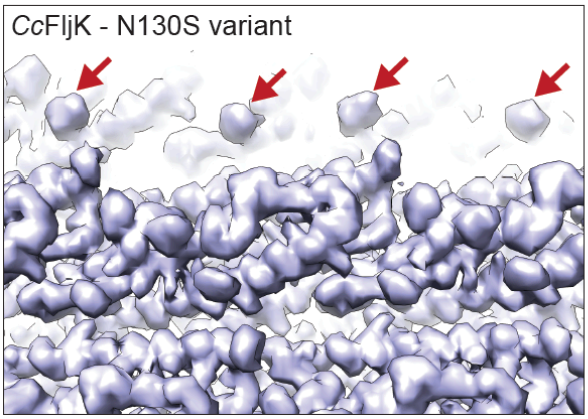
*Cc*FljK - N130S variant

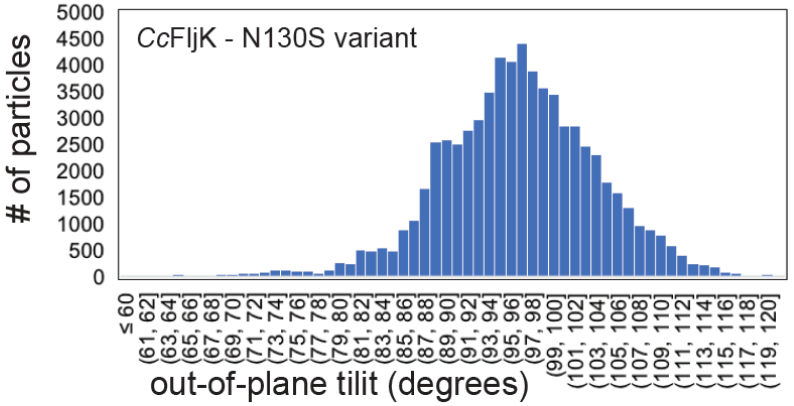
*Cc*FljK - N130S variant
# of particles
out-of-plane tilit (degrees)

C

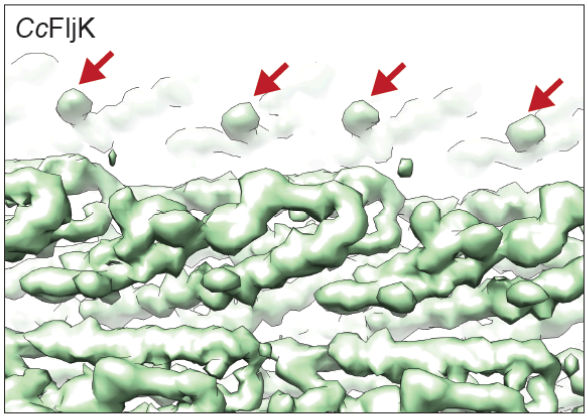
*Cc*FljK

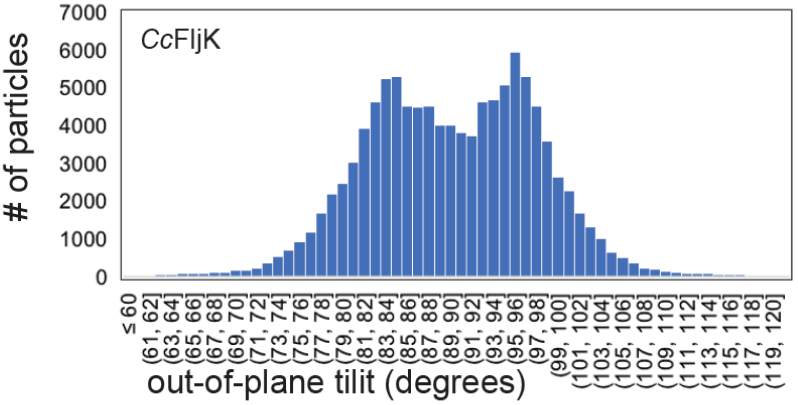
*Cc*FljK
# of particles
out-of-plane tilit (degrees)

D

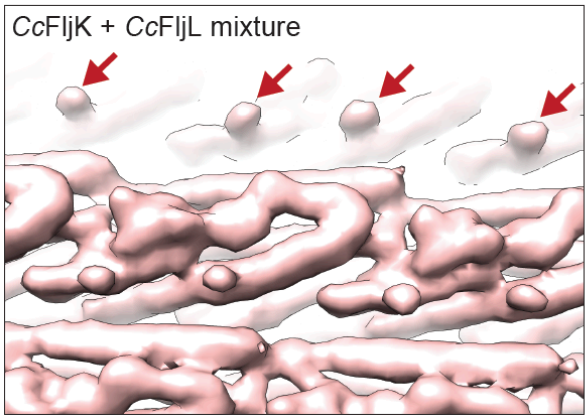
*Cc*FljK + *Cc*FljL mixture

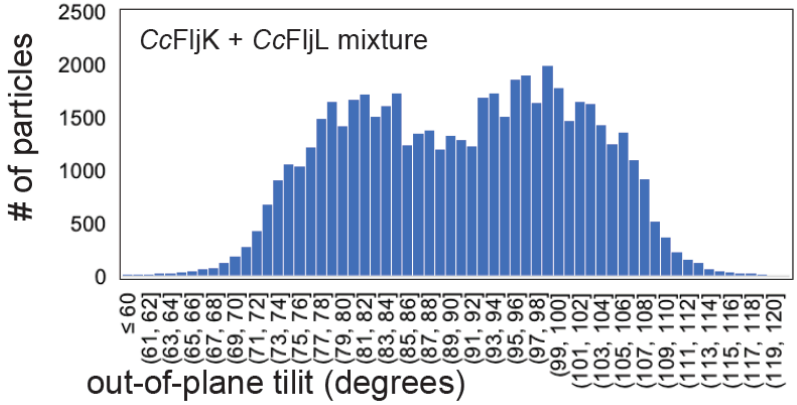
*Cc*FljK + *Cc*FljL mixture
# of particles
out-of-plane tilit (degrees)

Supplementary Figure 6. Out-of-plane tilt analysis of helical reconstructions. Small red arrows denote threonine glycosylation sites observed in the higher resolution FljK maps (Fig. 5E). A) Deliberate application of likely incorrect helical symmetry during map reconstruction in Relion 3.1 returns a nonsensical map. Comparison of the resulting out-of-plane tilt values for the refined particle stack shows a pronounced bi-modal distribution. B) In contrast, use of estimated helical symmetry from Relion 3.1 yields a map with clearly defined protein secondary structure and an out-of-plane tilt distribution that is approximately gaussian. C.D) A similar analysis on the non-straightened reconstructions of FljK with or without FljL shows a near gaussian distribution with a small central dip that likely arises from the non-straightened nature of these filaments, and therefore non-ideal application of helical symmetry about a linear helical axis in Relion 3.1.

SUPPLEMENTARY REFERENCES

1. Egelman EH. 2010. Reconstruction of helical filaments and tubes. Methods Enzymol 482:167-83.
2. Isaacs N. 2016. A history of experimental phasing in macromolecular crystallography. Acta Crystallogr D Struct Biol 72:293-5.
3. Evans P, McCoy A. 2008. An introduction to molecular replacement. Acta Crystallogr D Biol Crystallogr 64:1-10.
4. Rossmann MG. 2001. Molecular replacement--historical background. Acta Crystallogr D Biol Crystallogr 57:1360-6.
5. He S, Scheres SHW. 2017. Helical reconstruction in RELION. J Struct Biol 198:163-176.
6. Blum TB, Filippidou S, Fatton M, Junier P, Abrahams JP. 2019. The wild-type flagellar filament of the *Firmicute Kurthia* at 2.8 Å resolution *in vivo*. Scientific Reports 9:14948.
7. Johnson MC, Kollman JM. 2020. Cryo-EM structures demonstrate human IMPDH2 filament assembly tunes allosteric regulation. Elife 9.
8. Wang F, Burrage AM, Postel S, Clark RE, Orlova A, Sundberg EJ, Kearns DB, Egelman EH. 2017. A structural model of flagellar filament switching across multiple bacterial species. Nature Communications 8:960.
9. Yamaguchi T, Toma S, Terahara N, Miyata T, Ashihara M, Minamino T, Namba K, Kato T. 2020. Structural and functional comparison of *Salmonella* flagellar filaments composed of FljB and FliC. Biomolecules 10.
10. Maki-Yonekura S, Yonekura K, Namba K. 2010. Conformational change of flagellin for polymorphic supercoiling of the flagellar filament. Nature Structural and Molecular Biology 17:417-422.